Nuclear Instruments and Methods in Physics Research A 1063 (2024) 169312

Contents lists available at ScienceDirect

Nuclear Inst. and Methods in Physics Research, A

journal homepage: www.elsevier.com/locate/nima

Operational experience and performance with the ATLAS Pixel detector at the Large Hadron Collider at CERN

James Philip Iddon, on behalf of the ATLAS Collaboration

CERN, Geneva, Switzerland

ARTICLE INFO

Keywords:
ATLAS
Detector operations
Radiation damage

ABSTRACT

In LHC Run 3, operating the ATLAS Pixel detector has been smooth, despite a typical number of interactions per bunch crossing of 62 in proton–proton collisions and after reaching fluence of $\mathcal{O}(10^{15})$ 1 MeV n-eq cm^{-2}. This contribution will detail the adjustments and improvements made to both the detector configuration and to the DAQ system respectively, necessary for keeping the performance of the ATLAS Pixel detector high as the operating conditions become more demanding, as well as results from radiation damage studies, their effect on operational parameters, and the subsequent outlook for the remainder of Run 3.

1. Introduction

As the innermost tracking system of ATLAS [1], the Pixel Detector is primarily responsible for vertexing, and it also provides dE/dx measurements for charged particles. Pixel comprises four barrel layers from radii 3.35 cm to 12.25 cm with an active area of 1.6 m^2, as well as three endcap disks on either side with an active area of 0.28 m^2. The innermost barrel layer, known as Insertable B-Layer (IBL) [2], was inserted in 2014 during the LHC Long Shutdown 1. IBL consists of 200 μm thick n+-on-n planar sensors as well as 230 μm thick n+-on-p 3D sensors in the outermost positions on the stave, bump-bonded to Front End (FE) FE-I4 chips in 130 nm CMOS, each with 26,880 pixels with a pitch of 50 × 250 μm^2 and 4 bit Time-Over-Threshold (TOT). The remainder of Pixel (referred to as 'original Pixel' [3]) has been operational since the beginning of LHC Run 1, and uses 250 μm thick n+-on-n planar sensors, with FE-I3 chips in 250 nm CMOS, each with 2880 pixels with a pitch of 50 × 400 μm^2 and 8 bit ToT. In Pixel, a module is 16 FE-I3 plus one Module Controller Chip (MCC), whilst in IBL a module is defined as two FE-I4. IBL and original Pixel are radiation hard to a dose of 250 Mrad and 50 Mrad respectively, or 5×10^{15} 1 MeV n-eq cm^{-2}(1×10^{15} 1 MeV n-eq cm^{-2}) fluence equivalent.

LHC Run 3, ongoing since spring 2022, is the last LHC run where Pixel, and the rest of the current inner detector, will be active, before being replaced by ITk [4,5] for Run 4. The goal of Run 3 is to collect twice as much integrated luminosity as was recorded in Run 1 and Run 2 combined, necessitating a high average number of interactions per bunch crossing, or pile-up (μ).

The relevant parameters affecting detector performance are trigger rate as well as instantaneous luminosity and pile-up. The pile-up conditions are characterised by the peak $\langle\mu\rangle$ per fill where $\langle\mu\rangle$ is the average pile-up over a lumi-block, and a lumi-block is a unit of time of up to 60 s. A typical fill in 2022 had a peak $\langle\mu\rangle$ of 52 and in 2023 of 62. Pixel also has to contend with the effects of radiation damage, reaching a fluence of $\mathcal{O}$ (10^{15}) 1 MeV n-eq cm^{-2}, at the limit of design fluence for B-Layer. The detector configuration and DAQ improvements that have made it possible for Pixel to operate in these demanding conditions will be outlined in this contribution.

2. Operational challenges and mitigations

Original Pixel was designed to cope with a peak $\langle\mu\rangle$ of 23. In typical proton–proton fills for Run 3, peak $\langle\mu\rangle$ measured by ATLAS was typically 52 in 2022 and 62 in 2023, a factor ≈ 3 above original Pixel design. A high $\langle\mu\rangle$ increases digital activity on the FE, resulting in an increase in the amount of data to read out, as well as a noticeable increase in digital current in FE-I3. In addition, the effects of Single Event Effects (SEEs) in FE-I4 become more apparent, resulting in an increase in quiet and noisy pixels.

2.1. Smart L1 forwarding

Modules can handle up to 16 triggers synchronously, due to limited buffer size. Exceeding this limit causes the module to become desynchronised with the Level-1 trigger stream until the next ATLAS Event Counter Reset (ECR), which is issued during a 2 ms pause in the L1 trigger stream every 5 s, used by ATLAS for system re-synchronisation. The events until the ECR become unusable because the Bunch Crossing Identifier (BCID) or Level-1 Identifier (L1ID), both forwarded by the MCC, are not synchronised with the corresponding

E-mail address: james.philip.iddon@cern.ch.

https://doi.org/10.1016/j.nima.2024.169312
Received 8 February 2024; Received in revised form 28 March 2024; Accepted 1 April 2024
Available online 2 April 2024

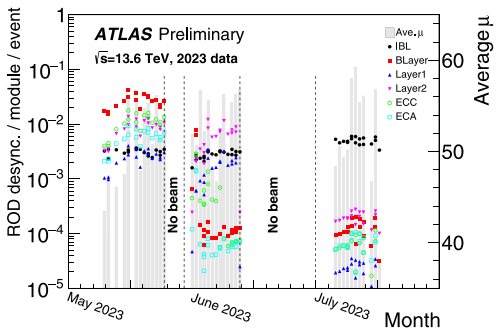

Fig. 1. The average fraction of Pixel modules with ROD level desynchronisation per event in 2023 runs. Each point shows the average fraction in a given run. Smart L1 FW was deployed in stages for different Pixel layers. From July onwards, it was deployed throughout the entirety of Pixel. Smart L1 FW for IBL is still under development. The average μ in the plots show μ averaged over an entire run.
Source: From [6].

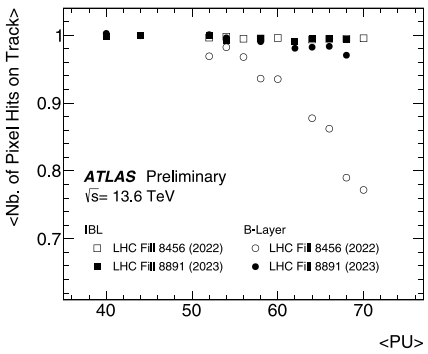

Fig. 2. Average number of pixel hits on the IBL (squares) and B-Layer (circles) associated to reconstructed particle tracks with pT > 0.7 GeV as a function of <PU>, or $\langle\mu\rangle$. Data were collected during dedicated fills in 2022 (LHC fill 8456, shown by the open markers) and 2023 (LHC fill 8891, shown by the filled markers), where the values of $\langle\mu\rangle$and trigger rate were scanned to study the detector response.
Source: From [8].

values held by the ReadOut Driver (ROD). The effect is called ROD level desynchronisation.

Smart L1 Forwarding firmware (Smart L1 FW), loaded in the ROD, keeps track of the number of pending triggers for each module. If the number of pending triggers exceeds the buffer size of the module, a new trigger is not sent, and a dummy fragment is inserted into the data stream to stay synchronised with the L1ID. This mechanism results in the loss of a some events which are discarded whilst the MCC processes events already in its buffer, but stays in sync with the L1ID by tagging in the event stream for proper reconstruction. As a consequence, significantly fewer events are lost compared to ROD level desynchronisation until the next ECR. As seen in Fig. 1, the ROD level desynchronisation decreases by two orders of magnitude from May 2023, where Smart L1 FW was not installed, to July 2023, where Smart L1 FW was installed everywhere in original Pixel.

2.2. Raised B-layer thresholds

When FE activity is high, single FEs within a module can lose synchronisation with the BCID of the MCC, known as module level desynchronisation, leading to unusable events until the next ECR. By raising the charge threshold, FE activity and therefore module level desynchronisation can be reduced. Conversely, charge thresholds need to be decreased to account for loss in Charge Collection Efficiency (CCE) with increased charge trapping due to radiation damage. The most appropriate charge threshold is a compromise the two effects.

A high module level desynchronisation in B-Layer was observed at the beginning of Run 3, correlated to the increase in peak $\langle\mu\rangle$ from a typical value of 52 in Run 2 to 62 in Run 3. The B-Layer thresholds were raised in response, from 3500 e^- to 4700 e^-, with the subsequent decrease in FE activity resulting in a factor two reduction in the number of modules desynchronised per event, and a factor roughly five reduction in the ATLAS deadtime contribution from Pixel, from $\approx$ 2% to $\approx$ 0.4% in typical *pp* fills.

2.3. Reconfiguration at ECR

FE-I4 are subject to SEEs in global and pixel registers. Single Event Upsets (SEUs) and Single Event Transients (SETs) in global registers can cause the FE-I4 to become silent or noisy, and to experience sudden changes in current consumption. Since Run 2, the effects of SEUs and SETs in global registers have been addressed, by re-configuring global registers every ECR. The reconfiguration of global registers has eliminated the problems of dead or noisy FEs, and the resulting changes in current consumption.

SEUs and SETs in pixel registers can cause the pixel to become noisy or unresponsive, with the number of noisy or dead pixels accumulating over the course of a fill. The reconfiguration every ECR was extended to pixel registers in IBL at the end of Run 2 in dedicated test fills, and shown to appreciably reduce the effect of SEUs and SETs [7]. Reconfiguration on a pixel level every ECR was deployed fully in IBL in 2023. Since the ECR is only 2 ms, only a subsection of pixels can be re-configured each ECR. Therefore, a subsection of pixels are reconfigured on a rolling basis each ECR, such that each pixel register is reconfigured once every 11 min. A significant reduction in the number of noisy or quiet pixels is observed after the introduction of the mechanism to IBL, with no additional deadtime to ATLAS since the reconfiguration occurs within the 2 ms ECR gap.

2.4. Probing operational limits

In both 2022 and 2023, special LHC fills were performed where $\langle\mu\rangle$ and L1 trigger rate were scanned, and used to study the response of the detector. The difference in the two fills was the inclusion of the reconfiguration on a pixel level at ECR in IBL, Smart L1 FW in Pixel, and raised B-Layer thresholds in 2023 and the lack of these developments in 2022. The average number of pixel hits associated to particle tracks with pT > 0.7 GeV is shown in Fig. 2. The improvement in the response of B-Layer is significant. Without Smart L1 FW and raised thresholds, B-Layer could maintain a hit-on-track efficiency of > 96% if $\langle\mu\rangle$ was below 57. At $\langle\mu\rangle$ of 62, the typical value in 2023, the hit-on-track efficiency of B-Layer was only 90%. However, with Smart L1 FW and raised thresholds, B-Layer maintains a hit-on-track efficiency > 96% until the maximum $\langle\mu\rangle$ reached in the 2023 fill of 68.5, with a hit-on-track efficiency of 98% at the typical $\langle\mu\rangle$ in 2023 of 62.

The hit-on-track efficiency of IBL remains consistent between the 2022 and 2023 fills, where the difference is the inclusion of pixel level reconfiguration every ECR in 2023, because SEEs on a pixel level are unlikely to affect entire clusters.

3. Radiation damage studies

The main effects of bulk damage are seen in modifications to charge collection properties due to the generation of electrically active defects. These modifications include an increase in leakage current, a change in depletion voltage due to changes in effective doping concentration, as well as a decrease in CCE and spatial resolution due to signal reduction caused by charge trapping.

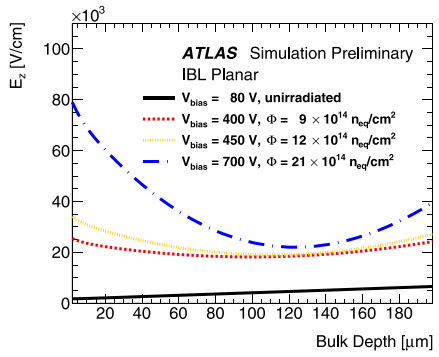

Fig. 3. E-field distribution along bulk depth for IBL planar sensors, simulated with TCAD. Electrons drift towards lower values of bulk depth. The fluences (Φ) and bias voltages (V_{bias}) presented correspond to the beginning of Run 2 (unirradiated, $V_{bias} = 80$ V), the end of Run 2 ($\Phi = 9 \times 10^{14}$ 1 MeV n-eq cm^{-2}, $V_{bias} = 400$ V), end of 2023 *pp* program ($\Phi = 12 \times 10^{14}$ 1 MeV n-eq cm^{-2}, $V_{bias} = 450$ V), and projection for the end of Run 3 ($\Phi = 21 \times 10^{14}$ 1 MeV n-eq cm^{-2}, $V_{bias} = 700$ V).
Source: From [13].

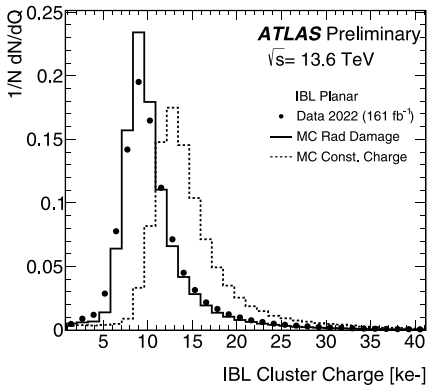

Fig. 4. Cluster charge Landau distribution at bias voltage of 450 V corrected by particle path in silicon after accumulating 161 fb^{-1} of integrated luminosity, corresponding to the beginning of Run 3.
Source: From [14].

A radiation damage digitiser simulating charge collection with E-field distributions at varying fluences and bias voltages has been developed by ATLAS [9], and used by default in the official ATLAS Run 3 MC simulation. The radiation damage effects are simulated in TCAD using the Chiochia model [10], for planar sensors, and the LHCb model [11] for 3D sensors, generating the E-field, Lorentz angle and Ramo potential distributions which are input to the ATLAS Run 3 MC. For 3D sensors, the Lorentz angle is negligible because the E-field and B-field are almost parallel. The fluence value is extracted from leakage current data and averaged over the stave, weighted by the track density. In the ATLAS Run 3 MC, the collection time is calculated from the TCAD E-field profile and a carrier is denoted as trapped if the collection time is slower than a randomly generated trapping time [12]. If so, the perturbation to the E-field of the trapped charge carrier is calculated with the Ramo potential distribution.

The E-field profile as a function of bulk depth at example fluences and bias voltages is shown in Fig. 3. When unirradiated, the E-field profile is linear with bulk depth. The three irradiated cases shown are all after type inversion, which occurred at roughly 2×10^{13} 1 MeV n-eq cm^{-2} [9]. With increasing fluence, a minimum appears in the electric field in the centre of the bulk.

3.1. Charge collection efficiency

Fig. 4 shows the cluster charge Landau distribution of the IBL planar sensors after integrating 161 fb^{-1} of luminosity at a bias voltage of 450 V, corresponding to the beginning of Run 3. The ATLAS Run 3 MC prediction, including the radiation damage digitiser, has a Most Probable Value (MPV) within 1% of the MPV of data, whilst the constant charge MC, which does not account for the effects of radiation damage, significantly differs from data.

CCE is shown as a function of integrated luminosity and corresponding fluence in Fig. 5, for IBL planar, B-Layer and FBK 3D sensors, where CCE is the MPV of the cluster charge distribution, normalised to the cluster charge MPV for unirradiation sensors in over depletion. Gains in CCE can be seen when bias voltage and thresholds are adapted. By regularly adapting bias voltage and thresholds, CCE will be kept within $\approx$ 50% of its original value at the end of Run 3, keeping hit efficiency well above 97%, assuming 400 fb^{-1} integrated luminosity. With increasing integrated luminosity, the depletion voltage increases. The bias voltages are evaluated each year such that they are sufficiently larger than the depletion voltage, ensuring the sensors are biased beyond depletion for at least the full year. Beyond the depletion voltage, only a minor gain in charge collection is seen.

3.2. 3D sensor performance

25% of the active area of IBL, ≈ 0.04 m^2, uses 3D sensor technology. 3D sensors use column electrodes passing through the silicon substrate, instead of planar electrodes sitting on top of the silicon substrate. Two different types of 3D sensors are used [16], FBK with columns that pass through the entire sensor thickness of 230 μm, and CNM with 210 μm columns which stop roughly 15 μm from the opposite edge, leaving approximately 200 μm overlap between n+ and p+ electrodes. 3D sensors are intrinsically more resistant to the effects of bulk damage because of the reduced charge drift path and collection time, without reducing the thickness of active silicon traversed by a charged particle.

The CCE as a function of integrated luminosity and average fluence for IBL FBK 3D sensors can be seen in Fig. 5. At a fluence benchmark of 8×10^{14} 1 MeV n-eq cm^{-2}, IBL 3D sensors have a CCE roughly 10% higher than planar, and at a fluence benchmark of 10^{15} 1 MeV n-eq cm^{-2}, not yet reached in the outermost positions of IBL where the 3D sensors are located, a CCE 25%–30% higher is seen for IBL 3D sensors with respect to IBL planar [17] for the foreseen operating conditions.

4. Conclusions

Thanks to adjustments made to the configuration of the ATLAS Pixel Detector and the improvements made to its DAQ system, both software and firmware, operations in 2023 has been smooth, and the performance of Pixel for critical metrics such as hit-on-track efficiency remain sufficiently high despite the harsher operating conditions of LHC Run 3. The radiation damage Monte Carlo agrees with data remarkably well, over a two order magnitude range in fluence, and forecasts a reduction in charge collection efficiency by the end of Run 3 which will result in hit efficiency remaining greater than 97%. Despite operating in conditions only within a factor three to four of those forecast for HL-LHC inner trackers, Pixel is running well, and is foreseen to continue to do so until the end of Run 3, where it will be replaced by ITk. The innermost layers of ITk will use 3D sensor technology whose performance and resistance to bulk damage effects has been verified in the outermost positions of the IBL.

Declaration of competing interest

The authors declare that they have no known competing financial interests or personal relationships that could have appeared to influence the work reported in this paper.

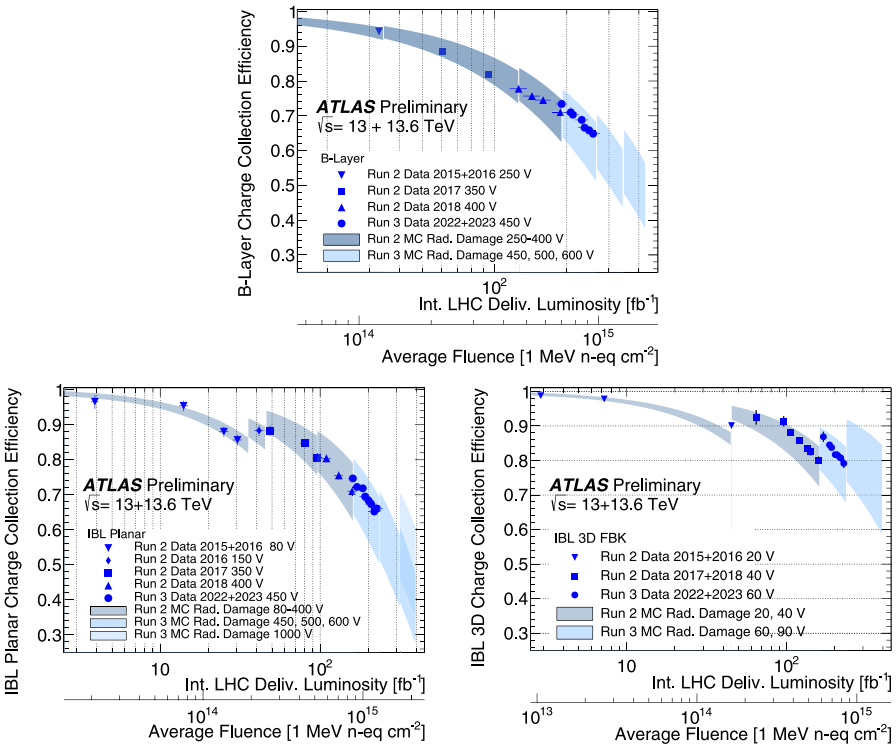

Fig. 5. Charge collection efficiency as a function of integrated delivered luminosity and average fluence for B-Layer (top), IBL planar (bottom left) and FBK 3D (bottom right) sensors, with the radiation damage MC shown by the bands in both cases. Fluence is extracted from leakage current data and averaged along the modules with the same longitudinal distribution as the particle tracks used in the analysis. Changes in CCE at the beginning of each year are due to yearly changes in bias voltage and thresholds, where the bias voltages are stated in the legend.
Source: From [15].

References

[1] The ATLAS Collaboration, The ATLAS experiment at the CERN Large Hadron Collider, JINST 3 (2008) S08003, http://dx.doi.org/10.1088/1748-0221/3/08/S08003.

[2] The ATLAS IBL Collaboration, Production and integration of the ATLAS Insertable B-Layer, J. Instrum. 13 (05) (2018) T05008, http://dx.doi.org/10.1088/1748-0221/13/05/T05008.

[3] G. Aad, et al., ATLAS pixel detector electronics and sensors, JINST 3 (2008) P07007, http://dx.doi.org/10.1088/1748-0221/3/07/P07007, URL https://cds.cern.ch/record/1119279.

[4] The ATLAS Collaboration, Technical Design Report for the ATLAS Inner Tracker Pixel Detector, Technical Report, CERN, Geneva, 2017, URL https://cds.cern.ch/record/2285585.

[5] The ATLAS Collaboration, Technical Design Report for the ATLAS Inner Tracker Strip Detector, Technical Report, CERN, Geneva, 2017, URL https://cds.cern.ch/record/2257755.

[6] The ATLAS Collaboration, Pixel ROD-level desynchronization in 2023, 2023, URL https://atlas.web.cern.ch/Atlas/GROUPS/PHYSICS/PLOTS/PIX-2023-004/. ATLAS-PIX-2023-004.

[7] G. Balbi, et al., Measurements of single event upset in ATLAS IBL, JINST 15 (06) (2020) P06023, http://dx.doi.org/10.1088/1748-0221/15/06/P06023.

[8] The ATLAS Collaboration, Pixel hit-on-track efficiency in 2023, 2023, URL https://atlas.web.cern.ch/Atlas/GROUPS/PHYSICS/PLOTS/PIX-2023-003/. ATLAS-PIX-2023-003.

[9] The ATLAS Collaboration, Modelling radiation damage to pixel sensors in the ATLAS detector, JINST 14 (06) (2019) P06012, http://dx.doi.org/10.1088/1748-0221/14/06/P06012.

[10] V. Chiochia, et al., A double junction model of irradiated silicon pixel sensors for LHC, NIMA (ISSN: 0168-9002) 568 (1) (2006) 51–55, http://dx.doi.org/10.1016/j.nima.2006.05.199.

[11] A. Folkestad, K. Akiba, M. van Beuzekom, E. Buchanan, P. Collins, E. Dall'Occo, A. Di Canto, T. Evans, V. Franco Lima, J. García Pardiñas, H. Schindler, M. Vicente, M. Vieites Diaz, M. Williams, Development of a silicon bulk radiation damage model for Sentaurus TCAD, Nucl. Instrum. Methods Phys. Res., A 874 (2017) 94–102, http://dx.doi.org/10.1016/j.nima.2017.08.042.

[12] M. Bomben on behalf of the ATLAS Collaboration, Including Radiation Damage Effects in ATLAS Monte Carlo Simulations: Status and Perspective, Technical Report, CERN, Geneva, 2023, URL https://cds.cern.ch/record/2876938. EPS-HEP2023 conference.

[13] The ATLAS Collaboration, TCAD field profile in IBL planar modules, 2023, URL https://atlas.web.cern.ch/Atlas/GROUPS/PHYSICS/PLOTS/PIX-2023-006/. ATLAS-PIX-2023-006.

[14] The ATLAS Collaboration, IBL radiation damage simulation, 2023, URL https://atlas.web.cern.ch/Atlas/GROUPS/PHYSICS/PLOTS/PIX-2022-002/. ATLAS-PIX-2022-002.

[15] The ATLAS Collaboration, Pixel charge collection efficiency, 2023, URL https://atlas.web.cern.ch/Atlas/GROUPS/PHYSICS/PLOTS/PIX-2023-001/. ATLAS-PIX-2023-001.

[16] The ATLAS IBL Collaboration, Prototype ATLAS IBL modules using the FE-I4A front-end readout chip, JINST 7 (11) (2012) P11010, http://dx.doi.org/10.1088/1748-0221/7/11/P11010.

[17] M. Battaglia on behalf of the ATLAS Pixel Detector Collaboration, ATLAS Planar and 3D Pixel Sensor Performance and Operational Experience at the Large Hadron Collider, Technical Report, CERN, Geneva, 2023, URL https://cds.cern.ch/record/2878403. EPS-HEP2023 conference.